Destruction of Amyloid Fibrils by Graphene through Penetration and Extraction of Peptides

Zaixing Yang[1,‡], Cuicui Ge[1,‡], Jiajia Liu[1], Yu Chong[1], Zonglin Gu[1], Camilo A. Jimenez-Cruz[2], Zhifang Chai[1], and Ruhong Zhou [1,2,3] *

[1] School for Radiological and Interdisciplinary Sciences (RAD-X), Collaborative Innovation Center of Radiation Medicine of Jiangsu Higher Education Institutions, and Jiangsu Provincial Key Laboratory of Radiation Medicine and Protection, Soochow University, Suzhou 215123, China

[2] IBM Thomas J. Watson Research Center, Yorktown Heights, NY 10598, USA

[3]Department of Chemistry, Columbia University, New York, NY 10027, USA

‡ These authors contribute equally

*Corresponding author, E-mail: ruhongz@us.ibm.com

Context:

PS1: Other representative trajectories for all the four types of simulated models with double or single graphene nanosheets.

PS2: Instruction to the video.

PS3: Two representative trajectories to show graphene sheet(s) spontaneously penetrating into the fibril.

PS4: One representative trajectory to show a larger graphene nanosheet spontaneously penetrating into the fibril with subsequent peptide extraction.

PS5: Role of interfacial water in assisting graphene's penetration into fibril.

PS6: Time evolution of the interaction potential energy illustrating the step-wise decrease upon lipid extraction

PS7: Potential of mean force for the estimate of binding free energy.

PS8: AFM images of s-GO and GO.

PS9: Sketches of restraints in all four types of simulated systems.

Supporting Information

PS1: Other representative trajectories for all the four types of simulated models with double or single graphene nanosheets.

Fig. S1 A and B show similar trajectories as shown in **Fig. 1** in the main text, but with additional runs (i.e., the two graphene nanosheets either attacking from the same side (Fig. S1A) or from both sides (Fig. S1B)). Again, both are shown to be capable of disrupting the preformed amyloid fibril through insertion/cutting and the direct extraction. Fig. S1C represents a typical trajectory of a single graphene nanosheet attacking from the edge, similar to that in the "docking" simulation in Fig. 2 of the main text. Again, the extraction of peptides is commonly seen. Fig. S1D shows a single graphene nanosheet attacking from the middle of fibril. The graphene can still cut into and extract peptides from the fibril. All these results indicate that the destruction mechanism with both insertion/cutting and direct extraction is very robust.

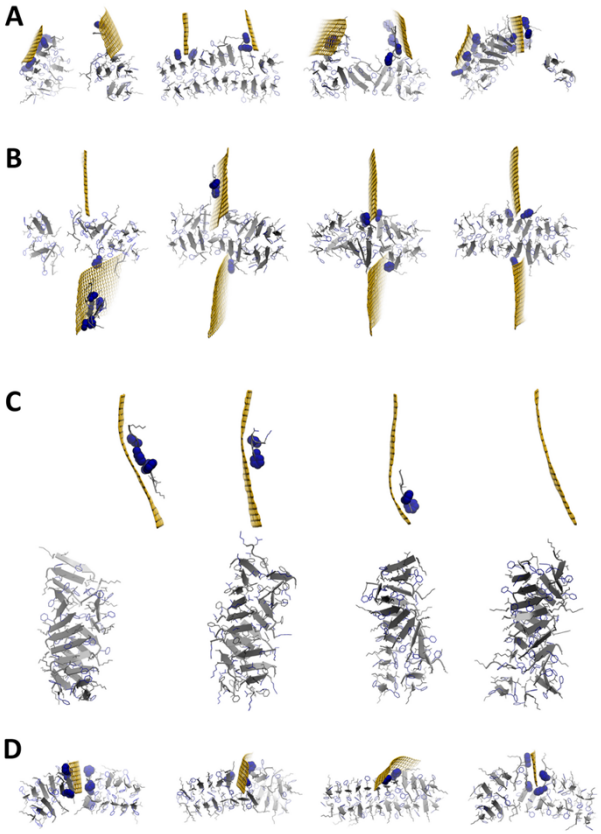

Fig. S1. The additional representative trajectories of graphene nanosheet(s) interaction with mature fibrils for all the four simulated models, with (A) showing two graphene sheets attacking a preformed Aβ amyloid fibril from the same side, (B) the two graphene sheets attacking from both sides, (C) the "top-edge-restrained"

graphene nanosheet docked at the edge of the Aβ amyloid fibril extracting peptides, and (D) a graphene sheet attacking from the middle of fibril. The Aβ peptides (total 24 monomers) are shown in sticks, with the two aromatic residues Phe shown in dark blue. The graphene sheet is shown as an orange-bonded sheet. Extracted peptides are highlighted with their Phe residues shown in larger van der Waals spheres. Color settings are the same as in **Fig. 1**, in the main text.

PS2: Instruction to the video.

The video shows how the two graphene nanosheets, attacking from both sides of the fibril, insert/cut into the fibril and extract large amount of peptides in atomic details (for simplicity the solvent and ions were not shown).

PS3: Two representative trajectories to show graphene sheet spontaneously penetrating into the fibril.

Two sets of additional simulations have been performed to investigate whether graphene can still dissociate the amyloid or not once the constraints on the graphene and peptides are removed. Both the cases with double graphene sheets or single sheet were studied. As shown in the new Fig. S3A, for the double graphene sheets case, once the constraints were removed, one graphene sheet quickly penetrated into the fibril and cut it into two halves (graphene staying inside the fibril), while the other sheet laid on the fibril surface till the end of the simulation. For the single graphene case (see Fig. S3B), the graphene also quickly penetrated into the fibril and cut it into two halves, and stayed inside the fibril. The peptide extraction was not observed though in these simulations, probably partly due to the too small size used (thus not enough graphene surface for additional extracted peptides), and partly due to the fact that at least one sheet was laying flat on fibril surface, which also leaves no room for peptide extraction.

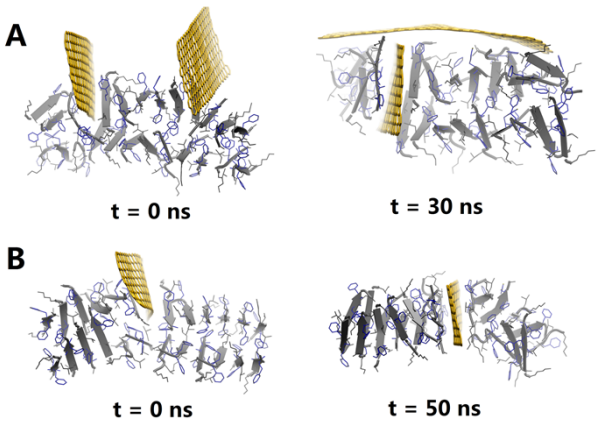

Fig. S3. Two representative trajectories to show graphene sheet spontaneously penetrate into the fibril; (A) for double graphene sheets, and (B) for single sheet attacking an amyloid fibril from the same side.

PS4: One representative trajectory to show a larger graphene nanosheet spontaneously penetrating into the fibril with subsequent peptide extraction.

To further illustrate the lipid extraction process, we doubled the size of the attacking graphene nanosheet in the constraint-free simulations. As shown in Fig. S4, after the graphene nanosheet (the right one) fully penetrated into the fibril at t = ~50 ns, the peptide extraction process started. At ~200 ns all the "hanging-out" portion of the inserted graphene was fully covered by the extracted peptides from fibril. This is also consistent with another very recent study where both the inserted bare and serum protein BSA-coated graphene nanosheets can extract lipids from cell membranes to their "hanging-out" portions, but with the BSA-coated one extracting less and covering only those available surfaces aside from BSA (Nanoscale, DOI: 10.1039/C5NR01839K, 2015).

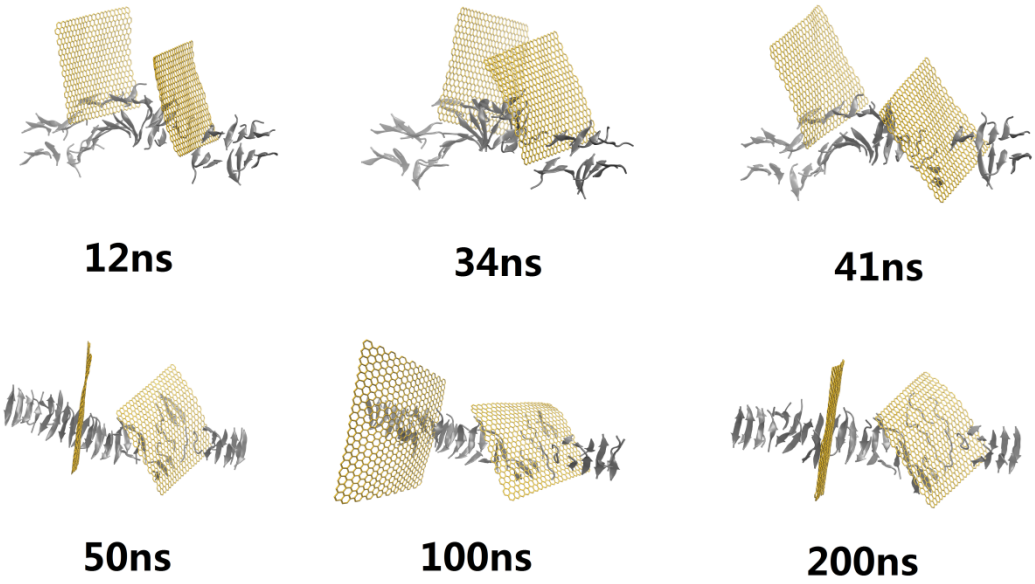

Fig. S4. One representative trajectory to show two graphene sheets spontaneously penetrate into the fibril, with the subsequent peptides extraction from the right graphene sheet. Other trajectories show the left graphene sheet extracts peptides first. If much longer simulations were performed, both graphene sheets will be covered by the extracted peptides eventually.

PS5: Role of interfacial water in assisting graphene's penetration into fibril.

The contributions of interfacial water between fibril and graphene to the processes of graphene's penetration can be described from the time evolution of the heavy atom contact number between graphene and fibril, as well as water solvation dynamics in the first solvation shell (FSS) for some representative residues, such as phenylalanine (aromatic) and lysine (basic) (Fig. S5). Initially, the sidechain of phenylalanine was buried in the hydrophobic core of fibril and remained dry. In this particular trajectory, as shown in Fig. S5, the β-sheet structure started to get ruptured around t=100 ns, due to the asynchronous adsorption of peptides onto the surface of graphene, and water molecules quickly intruded into fibril's hydrophobic core. At = 105 ns, the target phenylalanine was already solvated by ~11 water molecules. From ~110 ns to ~180ns, as graphene further penetrating into the fibril hydrophobic core, the heavy atom contact number between the sidechain and graphene increased from 0 to ~65, while the number of water molecules in FSS of Phe side chain dramatically decreased from ~18 to ~0. In other words, a fascinating dewetting (drying) phenomenon occurred at the interface between graphene and the hydrophobic cluster near the target phenylalanine, which provided a strong driving force for graphene's further penetration. It is noteworthy that during this drying process, the aromatic ring of

target phenylalanine is actually perpendicular to the graphene. As the simulation time progresses (after ~250 ns), the sidechain of the target phenylalanine climbed onto the surface of graphene, accompanied by rotating its aromatic ring to be parallel to the graphene surface, interestingly. This results in more aromatic ring atoms in contact with graphene, with the heavy atom contact number increased from ~65 to ~200, and thus a significantly strengthened π–π stacking interaction between graphene and phenylalanine. From then on, the target phenylalanine stayed in that conformation till to the end of the simulation, with both the heavy atom contact number and the number of water molecules in FSS nearly constant.

For lysine, on the other hand, its long sidechain (and especially the positive charged ε-amino group, NH_3^+) was fully solvated by ~18 water molecules (see the snapshot at t = 0 and 220 ns in Fig. S5) during the first ~250 ns of the simulation before it started to approach the graphene surface. Then, within a relatively short time interval from ~250 to ~300 ns, it was fully adsorbed onto the graphene surface. During this process, the heavy atom contact number between the side chain and graphene increased sharply from 0 to ~120, while the number of water molecules in its FSS only slightly decreased from ~18 to ~15 (see Fig. S5B), which is in contrast with the phenylalanine case.

Taken together, we can conclude that water molecules near the interface have played a significant role during the graphene insertion and peptide adsorption process. These water molecules have played at least two roles in this case: (i) to provide a strong driving force through final drying of hydrophobic residues, particularly phenylalanine, upon binding onto graphene; and (ii) to facilitate as a lubricant for basic residues, such as lysine, to bind to graphene.

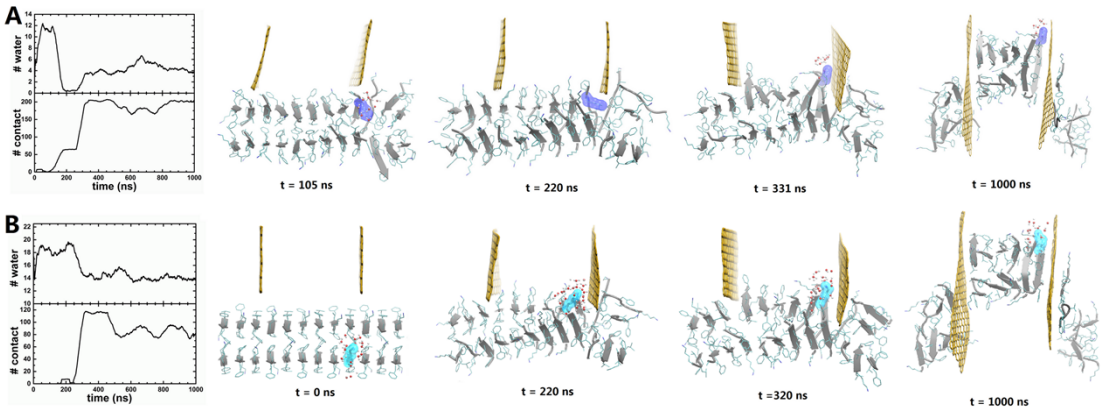

Fig. S5. The number of water molecules in first solvation shell (FSS) of Phe (A) and Lys (B) residues (top panel in the first graph), and the heavy atom contact number

between the residue and graphene (bottom panel in the first graph). The representative snapshots showing the local solvation of Phe (A) and Lys (B) are also shown. The red spheres represent the water oxygen atoms in FSS of target residue sidechain. The Aβ peptides (consisting of a total of 24 monomers) are shown in a cartoon representation, with the representative phenylalanine and lysine residues shown in blue and light blue surfaces. The graphene sheet is shown as an orange-flat-sheet.

PS6: Time evolution of the interaction potential energy illustrating the step-wise decrease upon lipid extraction

In addition to the PMF calculations, which clearly show the difference in binding energies (see Fig. S7), we also analyzed in detail the time evolution of the interaction potential energy changes to further illustrate this point. As shown in Fig. S6, two peptides with very similar positions with respect to the two graphene nanosheets were chosen to demonstrate their respective energy changes (step-wise decrease) once moving from the fibril to the graphene sheet. The interaction energies for peptide-1 and peptide-2 with fibril are about -48.16, and -52.56 kcal/mol; while they are -60.12 and -61.34 kcal/mol with graphene once extracted (Fig. S6C). Thus, the net interaction potential energy will be significantly lower by -11.96 and -8.78 kcal/mol, respectively, for peptide-1 and peptide-2, displaying a step-wise decrease upon extraction.

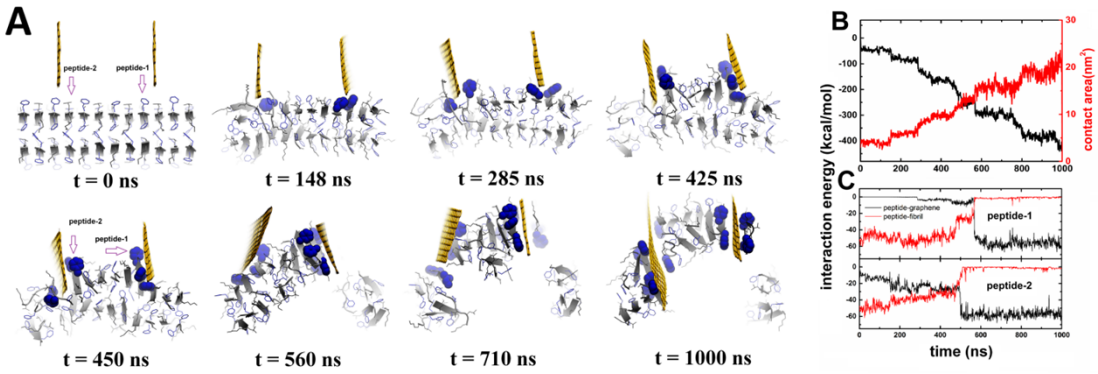

Fig. S6. (A) One representative trajectory showing the graphene nanosheet insertion and peptide extraction, featuring two graphene sheets attacking a pre-formed Aβ amyloid fibril from the same side (the same with the trajectory shown in Fig.1A in the main text). (B) Time evolution of the interaction potential energy between the graphene nanosheet and the peptide amyloid fibril (in black), alongside the contact area between the graphene and peptides (in red) for the trajectory. (C) The interaction potential energy between the peptide-1 (top panel) and peptide-2 (bottom panel) with

the graphene nanosheet (black) and fibril (red) as the function of simulation time, displaying a clear step-wise decrease in interaction potential energy once the peptide is extracted onto the graphene sheet.

PS7: Potential of mean force for the estimate of binding free energy.

Three sets of umbrella sampling simulations were performed to estimate the PMF for the peptide-fibril (from both interior and terminal) and peptide-graphene binding systems. Fig. S7 shows the sketches of these binding systems: (A) a peptide being pulled from the interior of the fibril, (B) a peptide being pulled from the terminal of the fibril, and (C) a peptide being pulled from the graphene surface. The peptide in green is the target peptide for pulling and the arrow indicates the pulling direction (PMF reaction coordinate). The PMF curves were obtained by using 25, 31 and 43 sampling windows along the reaction coordinates of the peptide in the interior, at the terminal of the fibril, and the peptide-graphene complex, respectively. The binding free energy for a peptide in the interior and at the terminal are calculated to be -16.34 kcal/mol and -8.24 kcal/mol (Fig. S7A-B), respectively. While it is -19.46 kcal/mol for the same peptide with graphene (Fig. S7C), which is about 3.12 and 11.42 kcal/mol more favorable than the peptide in the interior or at the terminal. These results further confirm that extraction of peptides from fibril to the graphene surface is energetically favorable.

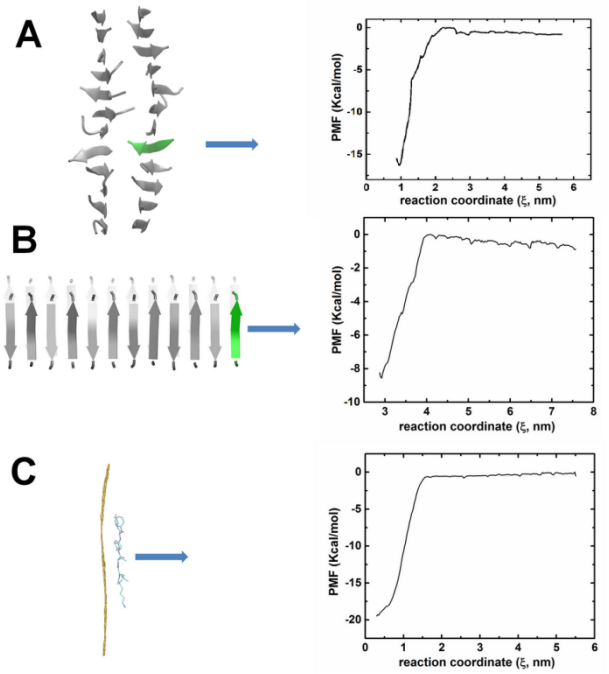

Fig. S7. The potential of mean force (PMF) calculations for the peptide KLVFFA being pulled from the interior (A) of the fibril, the terminal (B) of the fibril, and graphene surface (C). The left subfigure shows a sketch of the system, while the right subfigure shows the corresponding PMF. The peptide in green is the target peptide for pulling and the arrow indicates the pulling direction.

PS8: AFM images of s-GO and GO.

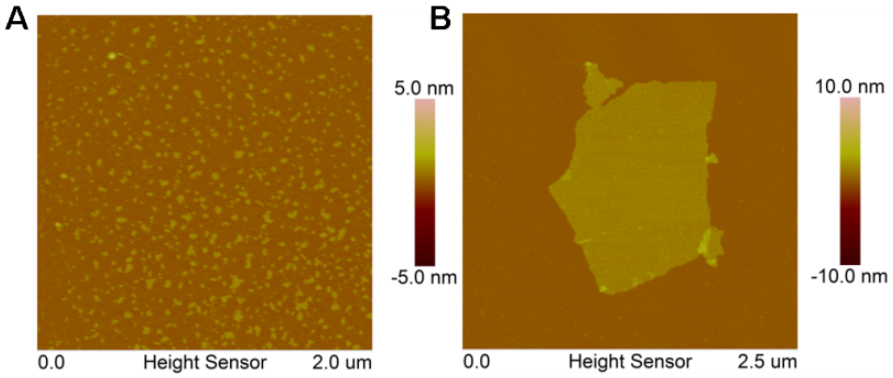

Fig. S8. AFM images of small sized graphene oxide (s-GO, with a lateral size <15 nm) (A), and normal sized GO with a lateral size of 0.5-3μm (B).

PS9: Sketches of restraints in all four types of simulated systems.

Fig. S9A-D show the sketches of restraints in all four types of simulated systems. All constrained atoms on graphene and peptide have been shown with large balls. Except for the graphene "docking" simulations, the positions of sixteen carbon atoms in four carbon rings at one of the corners were constrained by using a position restraint, while the other carbon atoms were left free to move. For the graphene "docking" simulations, the entire top row of 6-membered rings was restrained. The two Cα atoms at the two ends of the terminal four peptide chains in the β-sheet were also restrained, while the remaining peptides were allowed to move freely.

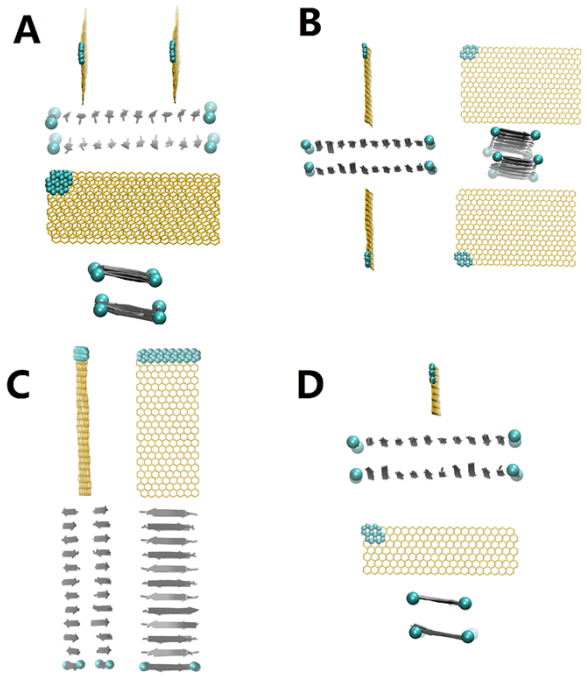

Fig. S9. A schematic picture of restrained atoms in all the four types of simulated systems. (A) two graphene sheets attacking a preformed Aβ amyloid fibril from the same side, (B) the two graphene sheets attacking from both sides, (C) the "top-edge-restrained" graphene nanosheet docked near the surface of the Aβ amyloid fibril, and (D) a graphene sheet attacking from the middle of fibril. All restrained atoms are shown in cyan vdW balls, graphene in orange-colored sheets, and Aβ peptides (consisting of a total of 24 monomers) in grey cartoon representations.